INES NOISE MODEL

N. Schartel[1], **P. Rodríguez-Pascual**[1,2]
[1] ESA IUE Observatory, Apartado 50727, 28080 Madrid, Spain
Affiliated with the Astrophysics Division, Space Science Department
ESTEC, the Netherlands
[2]Dept. Física, Universidad Europea de Madrid,
C/Tajo, Urb. El Bosque, 28670 Villaviciosa de Odón, Madrid, Spain

Abstract

The Noise Models used for extraction of IUE spectra within INES are described, and correlations between the "true" (independent) errors and the provided (not independent) errors are given.

Key words: detectors, Noise: general

1 Introduction

An estimate of the noise in IUE images is essential for extraction of spectra from SILO images at two portions. First, the cross-dispersion profile fitting requires a signal-to-noise ratio in order to perform weighted fits to the data. Second, the errors are propagated through the extraction procedure in order to establish errors for the final extracted fluxes.

Detailed studies of the noise of IUE low dispersion images are given by Ayres, (1990 and 1993). The characteristics of the noise in IUE images are strongly altered by the photometric linearization procedure via an intensity transfer function (ITF) and by the spatial resampling required to derive the low-dispersion image format. Therefore, we followed the approach of Kinney, Bohlin and Neill, 1991, and derived the noise models empirically from flat-field images. The signal and the corresponding noise of flat-field science observations are mainly produced by charged particle radiation. In addition UV-Flood images were used. Their signal and corresponding noise are caused by the light of the calibration lamps.

The model of Kinney A. L., Bohlin R. C. and Neill, 1991, and the first version of a noise model for the IUE Final Archive processing used third order polynomials to describe the standard deviation of flux numbers as a function of flux number for different wavelength bins. The wavelength-dependence of the four coefficients of these polynomials are then each represented by a third-order polynomial to allow a determination of the expected standard deviation of any pixel given its wavelength and observed flux number (FN).

In order to test the previous noise model for the IUE Final Archive, non-variable stars with many observations (> 70) having the same exposure time were used. Comparing

the standard deviation of the extracted fluxes with the mean given errors we found that the provided errors do not represent the "true" errors sufficiently well. The main reasons are: 1) The fitted polynomials were not only used to describe the measured data. They were also used in the region where no measured data are available to derive the noise model. This was done in order to establish the noise as a function of flux number for the whole FN range. Because many polynomials have a negative derivative for the highest measured flux numbers, lower noise is obtained for higher flux numbers in such regions. 2) The fitting of the coefficients of each polynomial with third order polynomials appears unable to represent the wavelength-dependence very well and causes large over- or under-estimation of the noise as function of wavelength for certain flux number regions. 3) The autocorrelation of neighbouring flux numbers is not considered.

In comparison to the first version of the noise model for the IUE Final Archive processing, we describe the standard deviation as a function of wavelength and flux number as smooth as possible but still conserving the inherent structure (compare caption 2). Especially, we restrict the extrapolations to polynomials of first order, which guarantee that higher FN values always show higher noise. Finally, a handling of the autocorrelation is provided in the third section.

2 Generation of Noise Model

The noise of IUE observations is modeled as a function of the flux numbers, FN, and the wavelength, λ. The models are based on measurements of mean flux numbers, $< FN >$, and the corresponding standard deviation, $\sigma(FN)$ for different parts of some hundreds of science and UV-Flood images.

In total 112 science observations and 241 UV-Flood images were used to derive a noise model for images of the LWP camera, 154 science observations and 18 UV-Flood images were the basis to establish the noise model for images taken with the LWR camera, and 290 science observations and 237 UV-Flood images were considered for the noise model of SWP data, respectively. The numbers of these images sorted by camera and by their type (science or UV-Flood) are given in Tables in the Appendix.

Every image is divided in parts according to wavelength and lines. In the wavelength direction the given increments were used without any further resampling of the data. In the line direction all data points provided by the UV-Flood images were used. For data taken from science observation the line ranges from 17 through 31 and from 39 through 64 were excluded, because the source spectrum is present in this area.

Because of the different size of the line intervals the chosen parts contain either 41 or 80 pixels. Within them all pixels flagged with a flag number below -256 were excluded. Pixels flagged below -256 belong to reseau marks or are saturated, and are not considered in the final extraction of the spectra. For the remaining sets of flux numbers the mean, $< FN >$, and its standard deviation, $\sigma\,(FN)$, were calculated, if more than six of the original pixels survived the described selections procedure. The points in Figure 1 show the derived standard deviation versus the determined average at a wavelength of 1652 $\mathring{A}$. No systematic difference was found between the UV-Flood and science images. Therefore, all data points were considered with the same weight in what follows.

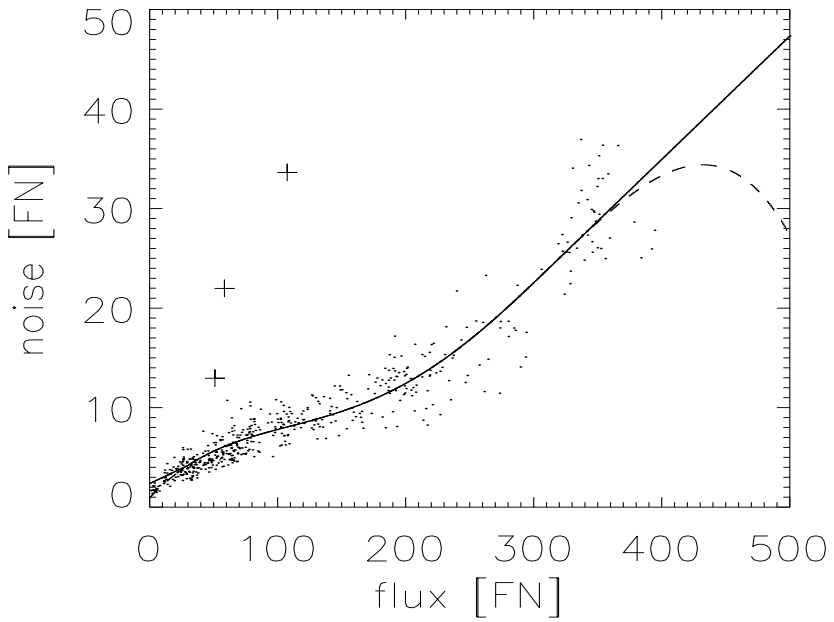

Figure 1: The dots represent the derived standard deviation, $\sigma\,(FN)$ over the corresponding median flux numbers $< FN >$ for a wavelength of 1652 $\mathring{A}$. The crosses indicate data values which were not considered for the modeling of the data. The continuously drawn line shows the finally accepted polynomials and the corresponding extrapolation. For comparison, the broken line shows the extrapolated polynomial.

For every wavelength step the standard deviation as a function of the FN value is described by polynomials of different order for different FN ranges. For FN values below thirty a first order polynomial was used in order to avoid boundary effects. In the FN range above thirty up to the point where still enough data points are available (breakpoint) a third order polynomial was fitted to the data taken with the LWP, and a fourth order polynomial was fitted to the data originating from the SWP and from the LWR, respectively. The data points collected for SWP observations show a larger curvature which requires a higher degree for the polynomial. The region of higher flux numbers are linearly extrapolated based on the third (fourth) order polynomial fit. Therefore, for a given wavelength, λ the noise, $\sigma\,(FN)$, is represented by:

$$\sigma\,(FN)|_{\lambda=const.} =$$

$$\begin{cases} B_1 + C_1 \cdot FN & for \quad FN \leq 30 \\ \sum_{i=0}^{4_{(SWP)},3_{(LWP)}} A_i \cdot FN^i & for \quad 30 \leq FN \leq breakpoint \\ B_2 + C_2 \cdot FN & for \quad FN > breakpoint \end{cases}$$

Cosmic events cause very high standard deviation for some of the collected $< FN >$-$\sigma\,(FN)$ data pairs. Therefore, we iterate the fitting of the third (fourth) order polynomial five times, excluding $< FN >$-$\sigma\,(FN)$-pairs for which $\sigma\,(FN)$ was greater then two times the values fitted in the previous iteration. By eye-inspection we checked that the mean of the distribution is well represented by the finally accepted fit, compare Figure 1.

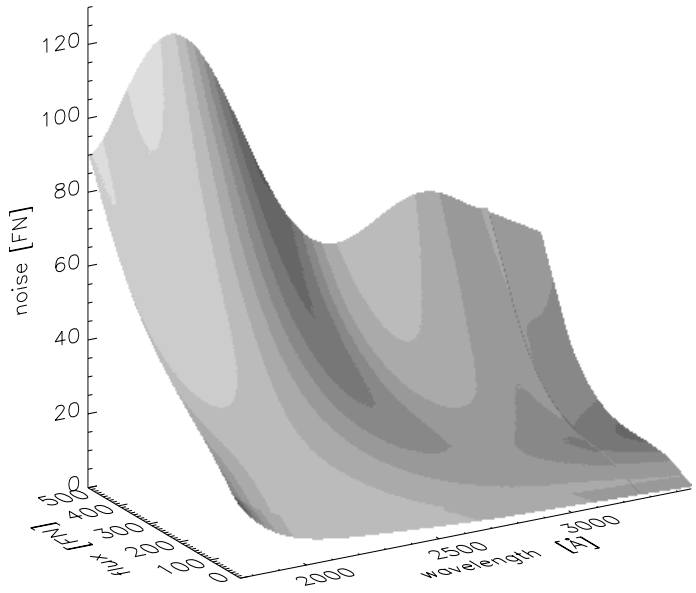

Figure 2: For the LWP camera observations the noise, in unit of flux numbers (FN), is shown over the two dimensional grid given by flux numbers and wavelengths.

The fitting and the corresponding extrapolation was done under the condition that a higher FN value must always show a higher noise level. Unfortunately, in about 10% of the wavelengths bins the highest FN values show a lower noise level in comparison to lower FN values and consequently the polynomials show a negative derivative. Therefore it was not possible to base the extrapolation simply on the highest obtained $< FN >$ values. This behavior was expected, because in some wavelength regions our images reach the saturation level, which causes a systematic reduction of the derived standard deviation. Therefore, we calculated the derivatite of the third (fourth) order polynomial for the 50 highest obtained $< FN >$ values and identified the breakpoint with that $< FN >$ value which showed the highest derivative. A different location of the breakpoint was found for the different analyzed wavelength steps. This mainly reflects the wavelength dependency of the sensitivity of the IUE cameras. For LWP data the breakpoints are located at flux numbers between 390 and 460 with a mean of 420. For the SWP we find a lower mean location of the breakpoint at a flux number of 335 covering the range from 280 to 400. The lowest mean location of the breakpoint was obtained for the LWR at a flux number of 175 covering a range between 105 and 410. These low flux numbers for the breakpoints are caused by the low number of UV-Flood images which can be used to derive the noise model for the LWR (compare Table 2 in the appendix). As a consequence of this the LWR noise model is based on extrapolations at a larger part as the models provided for the SWP or LWP.

The extrapolation is given by a straight line given through the breakpoint, the corresponding $\sigma\,(FN)$-value of the polynomial fit and the derivation of the polynomial at that point.

The same strategy, splitting in ranges and modeling with polynomials of different order, was used to smooth the models in the wavelength direction. Again, the order of the polynomial and the range where it is used was adjusted according to the given results from the

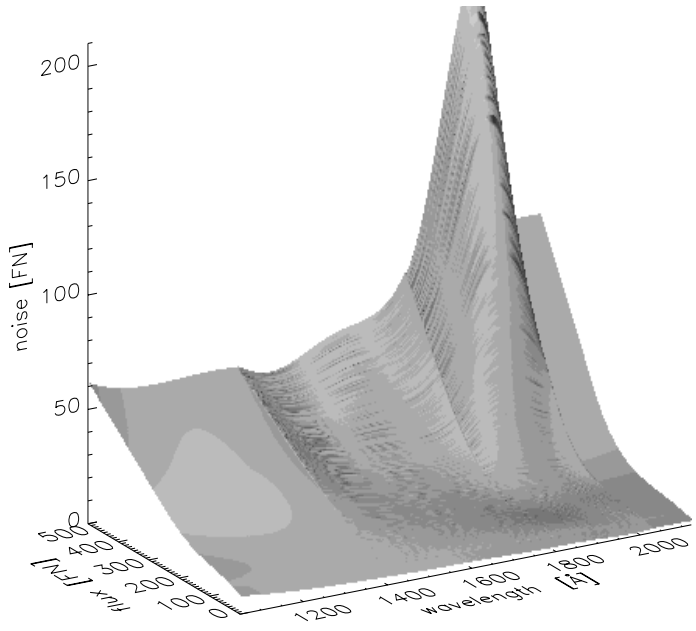

Figure 3: For the SWP camera observations the noise, in unit of flux number (FN), is shown over the two dimensional grid given by flux numbers and wavelengths.

fitting in the FN-direction. For the LWP camera the following ranges and corresponding order of polynomial were appropriate:

$$\sigma(\lambda)|_{FN=const.} = \begin{cases} \sum_{i=0}^{6} A_i \cdot \lambda^i & for \quad 1750\mathring{A} \leq \lambda \leq 3251\mathring{A} \\ \sum_{i=0}^{1} B_i \cdot \lambda^i & for \quad 3252\mathring{A} \leq \lambda \end{cases}$$

For LWR observations the following ranges and corresponding order of polynomial were chosen:

$$\sigma(\lambda)|_{FN=const.} = \begin{cases} \sum_{i=0}^{1} A_i \cdot \lambda^i & for \quad 1750\mathring{A} \leq \lambda \leq 1884\mathring{A} \\ \sum_{i=0}^{4} B_i \cdot \lambda^i & for \quad 1885\mathring{A} \leq \lambda \leq 3035\mathring{A} \\ \sum_{i=0}^{4} C_i \cdot \lambda^i & for \quad 3036\mathring{A} \leq \lambda \leq 3314\mathring{A} \\ \sum_{i=0}^{1} D_i \cdot \lambda^i & for \quad 3315\mathring{A} \leq \lambda \leq 3455\mathring{A} \end{cases}$$

Finally the following model was chosen for the SWP camera:

$$\sigma(\lambda)|_{FN=const.} =$$

$$\begin{cases} \sum_{i=0}^{3} A_i \cdot \lambda^i & for \quad 1050\mathring{A} \leq \lambda \leq 1502\mathring{A} \\ \sum_{i=0}^{6} B_i \cdot \lambda^i & for \quad 1503\mathring{A} \leq \lambda \leq 1801\mathring{A} \\ \sum_{i=0}^{3} C_i \cdot \lambda^i & for \quad 1802\mathring{A} \leq \lambda \leq 2023\mathring{A} \\ \sum_{i=0}^{1} D_i \cdot \lambda^i & for \quad 2024\mathring{A} \leq \lambda \end{cases}$$

In order to avoid large steps in the wavelength direction the fitting of the polynomial was always based on a larger range, overlapping with the next polynomial. Therefore, finally we derived the surface of the noise level above a two dimensional grid (1025×640) of flux numbers and wavelengths. The values in the FN direction of our grid covers a range from 0 to 1024. The step size in the wavelength direction is ≈2.6627 $\mathring{A}$ with a start point of 1750.0 $\mathring{A}$, resulting in a maximum wavelength of 3451.45 $\mathring{A}$ for the LWP images. The analogous values for the LWR are: 2.66573 $\mathring{A}$ (steps size), 1750.00 $\mathring{A}$ (start point) and 3453.40 $\mathring{A}$ (maximum wavelength), and for the SWP: ≈1.6763 $\mathring{A}$ (steps size), 1050.0 $\mathring{A}$ (start point) and 2121.18 $\mathring{A}$ (maximum wavelength), respectively.

During the photometric linearization of the raw data points a constant value is subtracted from the actual measurements. Consequently there are several line-by-line pixels with a negative value for short exposure times. Instead of providing a noise estimate for negative flux numbers the noise of such pixels is approximated with the noise of the zero flux number by fixed wavelength. This treatment is justified, because the negative flux numbers result from the scatter around the real zero value. The final derived noise is shown above the wavelength and the flux number in Figure 2 for the LWP camera and in Figure 3 for the SWP camera, respectively.

3 Provided error versus independent error

As mentioned above the noise models are required for the cross-dispersion profile fitting and for the error propagation during the extraction of the spectra from SILO images. These method was originally developed for analyzing CCD cameras, which provide a statistically independent flux for every pixel. In comparison to CCDs the IUE cameras are better considered as analogue instruments. Especially, the digital character of the pixels and the corresponding flux results from the read out procedure and subsequent analysis steps, rather than reflecting the physics of the detectors. As a consequence of this, a given flux number is not independent from the flux numbers obtained in its direct neighbourhood. The noise models obtained here consider this effect intrinsically, because they are based on measurements of flux numbers and the corresponding standard deviation from pixels which are direct "neighbour", compare section two. During the extraction of the spectra we propagate their error and these errors are these finally provided. They represent the statistic of the actual image and allow propagation through further analysis.

However, for may research activities a comparison of two or more observations of the same object is necessary. In such a case we are comparing spectra which are really statistically

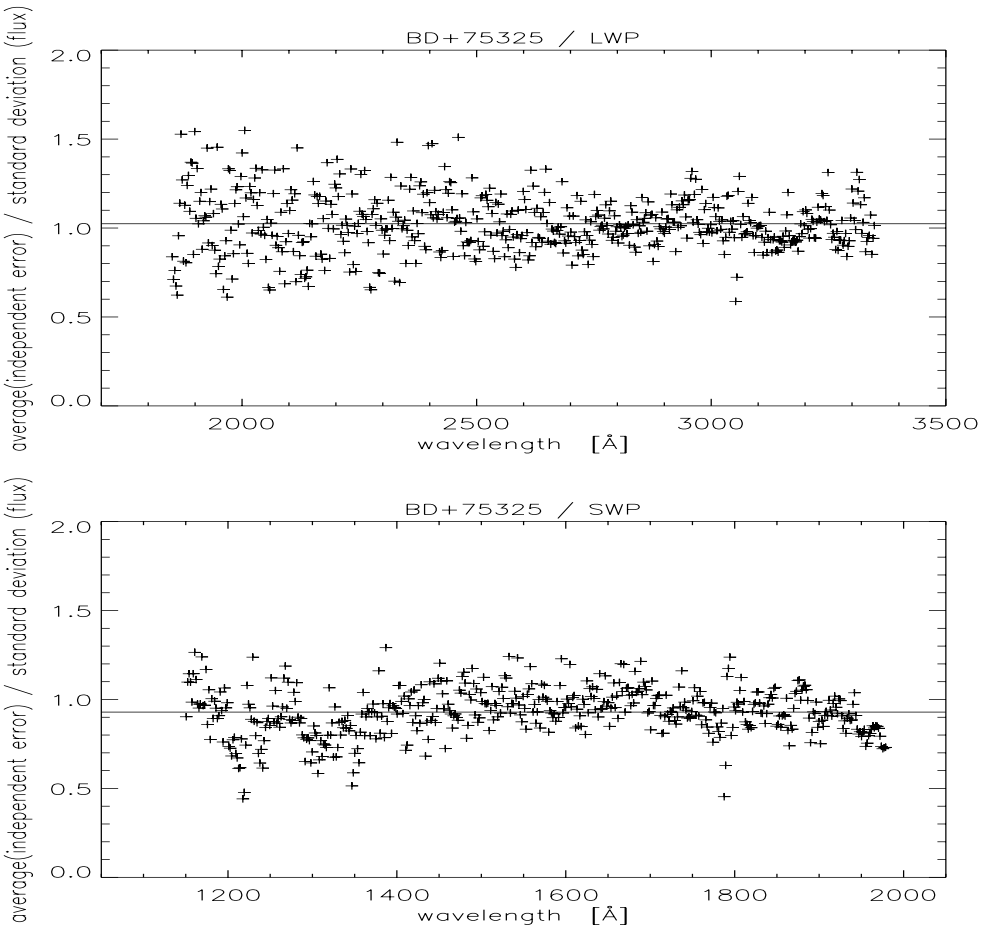

Figure 4: The ratios between the mean provided error and the standard deviation of the extracted fluxes are plotted as function of wavelength. The data are obtained for 70 LWP observations of BD+75325. In figure b the data result from 79 SWP observations.

independent. In order make use of the provided errors we have to establish a relation of the provided (statistically not independent) error with the statistically independent error.

To calibrate IUE and to determine the sensitivity degradation, several nonvariable stars were observed every year. In addition a substantial fraction of such calibration observations was performed with the same observation time. For BD+284211 in total 98 LWP observation are available with an exposure time of 49.848 s and 89 SWP observations with an exposure time of 25.674 s, respectively. With the extraction procedure we obtained flux measurements for every wavelength step of the LWP spectra, and for every wavelength steps of t he SWP, respectively. Because the star is not variable and the observations were performed with a fixed exposure time, the flux should be constant for a given wavelength. Therefore, the distribution and especially the standard deviation of the actually obtained fluxes are a measurement of the independent error. A comparison of the defined independent errors with the errors obtained via the error propagation was used to calibrate the relation of the provided (statistically not independent) error with the statistically independent error. For the LWP camera we get:

$$\sigma(flux)_{ind} = (0.35 + 0.00037 \cdot \lambda)\, \sigma(flux)_{prov}$$

where the wavelength, λ, is given in $\mathring{A}$ and $\sigma(flux)_{prov}$ is the error for the flux provided from the data extraction. For the LWR we have to consider two different equations depending on the UVC voltage under which the image were taken. For images taken with a voltage of -5.0 keV we get:

$$\sigma(flux)_{ind} = (1.37 - 0.00004 \cdot \lambda)\, \sigma(flux)_{prov}$$

and for a voltage of -4.5 keV the corresponding equation is:

$$\sigma(flux)_{ind} = (0.715 + 0.0001 \cdot \lambda)\, \sigma(flux)_{prov}$$

Images taken with the LWR camera are processed with two different ITFs (A-ITFs and B-ITFs), labeled with LWR83R94A and LWR83R96A in the comments of the images. Using images processed with the different ITFs we found that the provided equations hold for both in first order. Finally we get for the SWP camera:

$$\sigma(flux)_{ind} = (0.78 + 0.00029 \cdot w)\, \sigma(flux)_{prov}$$

In Figure 4a the ratios between the statistical independent error and the standard deviation of the extracted fluxes for BD+75325 are plotted as a function of the wavelength for the LWP observations. In Figure 4b the same is shown for the SWP images. The mean ratio over the whole wavelength range is 1.02 with a standard deviation of 0.16 for the LWP and 0.93 with a standard deviation of 0.13 for the SWP. Considering the standard deviation, the values are compatible with 1.0, the value expected for a correct treatment for statistically independent errors. Further the figures show no large systematic residuals, which indicate that there are no problematic areas in the noise models.

With the LWR camera a lower number of images were taken. In addition these have to be split according to the voltage with which the images were taken and according to the ITFs used to process them. Because of the smaller database the provided noise model as well as the provided correction equations do not reach the quality achieved for the SWP and LWP images. Therefore, depending on the flux numbers and the wavelength analyzed, systematic differences of up to 20% must be expected.

4 Discussion

Maybe the approach followed by Ayres (1990, 1993), to determine the noise in the raw image and to propagate the errors through the whole extraction procedure, is more obvious. This seems to be the case, especially, because the noise of the raw images can be understood

from a physical point to be a composite of read out noise and photon statistics. However, the data points derived from the images show no features which contradict the present method.

The restricted resources and the actual state of the final archive processing strictly requires a noise model for the SILO images already processed. Therefore, it was necessary to follow the approach of Kinney A. L., Bohlin R. C. and Neill, 1991. The same method was chosen to derive a first version of a noise model for the IUE Final Archive processing, see IUE New SIPS Information Manual, 1997, Chapter 9. In fact the same science images were used here.

There are no differences in the concept and the physical justification between the models described here and the previous two. But our description of the noise is more detailed. In the range where measurements of data points were available, different polynomials were fitted for different ranges which models the data significantly better than a third order polynomial. For the FN values where an extrapolation is necessary we restrict to a linear extrapolation and guarantee always that higher FN numbers show a higher noise level, which is not possible by extrapolating a higher order polynomial. We conserve the structure found above wavelength again by splitting in ranges and fitting different polynomials. This was not possible in the previous two models, because the interpolation in wavelength was done by fitting the constants of the polynomial as a function (third order polynomial) of wavelength.

A clear disadvantage of the new noise models is the size required to transport the information. The noise models are given in the form of three 3-dimensional FITS files which provide the noise for a given flux number and wavelength, whereas the old models need only 16 parameters to describe the flux number-wavelength-noise space. On the other hand because of the permanent increase of disk space and calculation speed of modern computers, the requirements necessary to make use of the new models is easily fulfilled. The files containing the new models will be public and will be distributed together with the Final Archive.

Access to noise models:

The three noise models are public and are included here as FITS files: LWP_noise.fits, LWR_noise.fits and SWP_noise.fits .

Acknowledgements. As mentioned in the discussion our work profited from previous studies and noise models for IUE. Therefore, we want to acknowledge, T. R. Ayres, A. L. Kinney, R. C. Bohlin, J.D. Neill and especially the Goddard IUE team. The latter created the first generation of noise models for the IUE final archive and supported our work by providing necessary input data.
Finally, we thank the Vilspa IUE team and especially Ian Skillen for very fruitful discussions.

References

Ayres T. R., 1990, PASP 102, 1420

Ayres T. R., 1993, PASP 105, 538

Kinney A. L., Bohlin R. C. and Neill J.D., 1991, PASP 103, 694

Garhart, M.P., Smith, M.A., Levay, K.L., Thompson, R.W., 1997, *'International Ultraviolet Explorer New Spectral Image Processing Information Manual–Version 2.0'*, see INES Document 3.2.9

Table 1: IUE images used to derive the noise models

Image numbers											
LWP / *Science images*											
01371	01374	01412	01414	01550	01565	01579	01603	01630	01647	01744	01752
01797	01798	01888	02247	02281	02310	02355	02417	02525	02537	02625	02836
02883	03067	03105	03232	03267	03268	03287	03379	03413	03457	03525	03534
03580	03698	03752	03828	03831	04103	04114	04116	04265	04445	04453	04546
04596	04599	04625	04626	04641	04680	04922	04944	04954	05026	05094	05100
05104	05197	05302	05353	05356	05357	05378	05382	05473	05708	05713	05873
06006	06058	06073	06168	06169	06178	06179	06180	06202	06203	06215	06216
06246	06247	06248	06262	06330	06407	06655	07433	07440	07453	07489	07654
07900	07901	08345	08711	08712	08732	08735	08736	08737	08955	11430	11561
11570	11571										
LWP / *UV-Flood images*											
01136	01137	01138	01140	01141	01142	01143	01144	01147	01148	01149	01150
01151	01152	01164	01166	01167	01171	01175	01182	01206	01208	01209	01212
01213	01214	01215	01226	01227	01228	01229	01234	01235	01236	01237	01238
01247	01248	01249	01270	01271	01272	01273	01275	01276	01277	01278	01300
01301	01302	01303	01305	01307	01314	01315	01316	01317	01318	01319	01327
01329	01330	01419	01420	01421	01422	01423	01424	01468	01469	01470	01471
01472	01473	01620	01621	01622	01623	01624	01625	01641	01643	01645	01646
01648	01721	01722	01723	01724	01725	01726	01894	01895	01896	01897	01898
01899	02049	02050	02051	02052	02053	02054	02523	03431	03432	03433	03434
03435	03436	04296	04297	04298	04299	04301	04302	04303	04334	04335	04337
04338	04340	04341	04342	04367	04368	04369	04370	04371	04372	04373	04374
04375	04376	04402	04403	04404	04405	04406	04407	04408	04409	04410	04411
04412	04426	04427	04428	04429	04430	04431	04432	04433	04434	04435	04817
04818	04819	04820	04821	06428	06429	06430	06431	06432	06433	07859	09299
09301	09302	09303	09304	10578	10579	10580	10581	10582	11779	11780	11781
11782	11783	11784	13024	13025	13026	13027	13028	13029	14397	14398	14399
14400	14401	14402	15180	15181	15182	15183	15184	15185	16622	16633	16634
16635	16636	16637	17610	17611	17612	17613	17614	17615	17663	17664	17665
17666	17667	17668	20214	20215	20217	20218	20219	20221	20222	20225	20226
20227	20228	20229	22065	22066	22067	22068	24416	24417	24418	24419	24420
24421											
LWR / *Science images*											
01582	01637	01638	01639	01640	01747	01748	01773	01775	01782	01786	01787
01803	02002	02050	02115	02213	02214	02230	02231	02258	02534	02745	02752
02815	02842	02960	02981	02982	03052	03089	03090	03124	03127	03617	03618
03974	04133	04351	04354	04410	04509	04511	04527	04530	04570	04596	04613
04616	04634	04635	04678	04680	04766	04948	05263	05956	06878	07635	07779
08046	08890	08896	08980	08981	09083	09122	09134	09458	09478	09519	10138
10366	10724	11111	11546	11637	11647	12078	12177	12219	12496	12508	12640
13008	13015	13025	13147	13501	13509	13510	13516	13517	13519	14090	14091
14324	14452	14532	14726	14812	15201	15270	15278	15348	15349	15350	15352
15353	15355	15365	15367	15426	15480	15485	15486	15496	15520	15757	15796
15817	16038	16432	16647	16679	16680	16856	16969	16975	17422	17433	17533
17574	17661	17755	17765	17923	17963	17977	18025	18112	18136	18201	18248
18297	18319	18357	18407	18440	18460	18552	18657	18735	18758		
LWP / *UV-Flood images*											
10311	16043	17427	17538	17970	17972	17973	18071	18137	18138	18139	18141
18197	18242	18243	18244	18246	18733						

Table 2: IUE images used to derive the noise models

Image numbers											
SWP / *Science images*											
01356	01361	01492	01498	01509	01802	01804	01805	01806	01894	01903	02099
02100	02148	02261	02394	03173	03212	03434	03554	03730	03731	03733	04292
04732	04929	04942	05116	05169	05376	05446	05455	05710	07444	07485	07486
07487	07491	07815	07981	08748	08749	08750	08881	08882	08884	08899	08900
08915	08916	09107	09258	09743	10058	10071	10090	10117	10312	10442	10460
10636	10683	10763	10832	10846	10952	10953	10954	13707	14476	14484	14485
14617	14651	15329	15535	15657	15673	15692	15773	15818	15822	16013	16423
16558	16715	16762	16763	16790	16801	16802	16803	16804	16816	16824	16836
16880	16884	16945	17077	17212	17219	17220	17228	17229	17230	17300	17301
17302	17303	17313	17393	17416	17517	17525	17659	18091	18328	18342	18427
18441	18457	18621	18662	18672	18673	18741	18772	18975	19048	19049	19074
19215	19216	19217	19223	19224	19238	19243	19252	19260	19301	19314	19321
19322	19448	19457	19671	19731	19805	19845	19846	19847	19858	19949	19995
19996	19997	19998	20003	20004	20058	20061	20071	20072	20073	20075	20084
20085	20112	20120	20142	20376	20706	20764	20816	20817	21185	21288	21296
21436	21459	21653	21654	21655	21662	21663	21664	21674	21675	21676	21694
21704	21921	22010	22184	22185	22204	22399	22400	22403	22874	22877	22878
22879	22880	22899	23144	23250	23319	23320	23443	23444	23451	23462	23617
23672	23691	23829	23892	23893	23996	24071	24075	24091	24099	24101	24185
24259	24580	24611	24768	24778	25257	25341	25355	25396	25496	25523	25551
25778	25798	25826	25827	25852	25873	25885	25892	25933	25973	25974	26132
26242	26411	26489	26506	26588	26734	26888	26889	26893	26894	26902	26911
27174	27189	27210	27211	27414	27424	27510	27517	27638	27639	27640	27704
27710	28072	28237	28257	28261	28304	28305	28346	28447	28469	28604	28750
28751	31860										
SWP / *UV-Flood images*											
02881	03142	03143	03145	03412	03433	03543	03570	04675	05021	05024	05025
05027	05454	05897	05900	05903	06072	06073	06074	06075	07033	07117	07118
07235	07237	07239	07251	07252	07253	07254	07273	07275	07277	08858	08859
09558	10419	10420	10422	13376	13378	13660	13685	13686	13688	14541	14789
14797	14814	15372	15373	15374	15375	15376	15377	16683	16684	16687	16864
16865	16866	16867	16868	16869	17540	17542	17543	17545	17546	17548	17734
17736	17737	17762	17992	17994	17995	18246	18588	18589	18590	18591	18592
18718	18719	19139	20107	20108	20109	20110	20111	20118	20151	20152	20153
21556	21557	21558	21559	21560	21561	22908	22909	22910	22911	22912	22913
24464	24465	24466	24467	24468	24469	25014	25015	25016	25017	25018	25019
25020	25021	25022	25024	25025	25056	25057	25058	25059	25060	25061	25062
25063	25064	25066	25067	25068	25092	25093	25094	25095	25097	25098	25099
25100	25101	25102	25103	25132	25133	25134	25135	25136	25137	25138	25139
25140	25141	25142	25143	25144	26432	26433	26434	26435	26436	26437	28016
28017	28018	28019	28020	28021	29501	29502	29503	29504	29505	29506	30643
30644	30645	30646	30647	30648	31959	31960	33385	33386	33387	33388	33389
33390	34146	34147	34148	34149	34453	34454	34455	34456	34457	34645	34646
34647	34648	34649	35867	35868	35869	35870	35871	35872	37595	37596	37597
37598	37599	37603	38755	38756	38757	38758	38759	38760	40188	41331	41332
41333	41335	41336	43453	46552	46553	46554	46555	46556			